



Supporting Online Material for

Helium and Neon Abundances and Compositions in Cometary Matter

Bernard Marty, Russell L. Palma, Robert O. Pepin,^{*} Laurent Zimmermann, Dennis J. Schlutter, Peter G. Burnard, Andrew J. Westphal, Christopher J. Snead, Saša Bajt, Richard H. Becker, Jacob E. Simones

^{*}To whom correspondence should be addressed. E-mail: pepin001@umn.edu

Published 4 January 2008, *Science* **319**, 75 (2008)
DOI: 10.1126/science.1148001

This PDF file includes:

Materials and Methods
SOM Text
Figs. S1 to S3
Table S1
References

Supporting Online Material

Materials

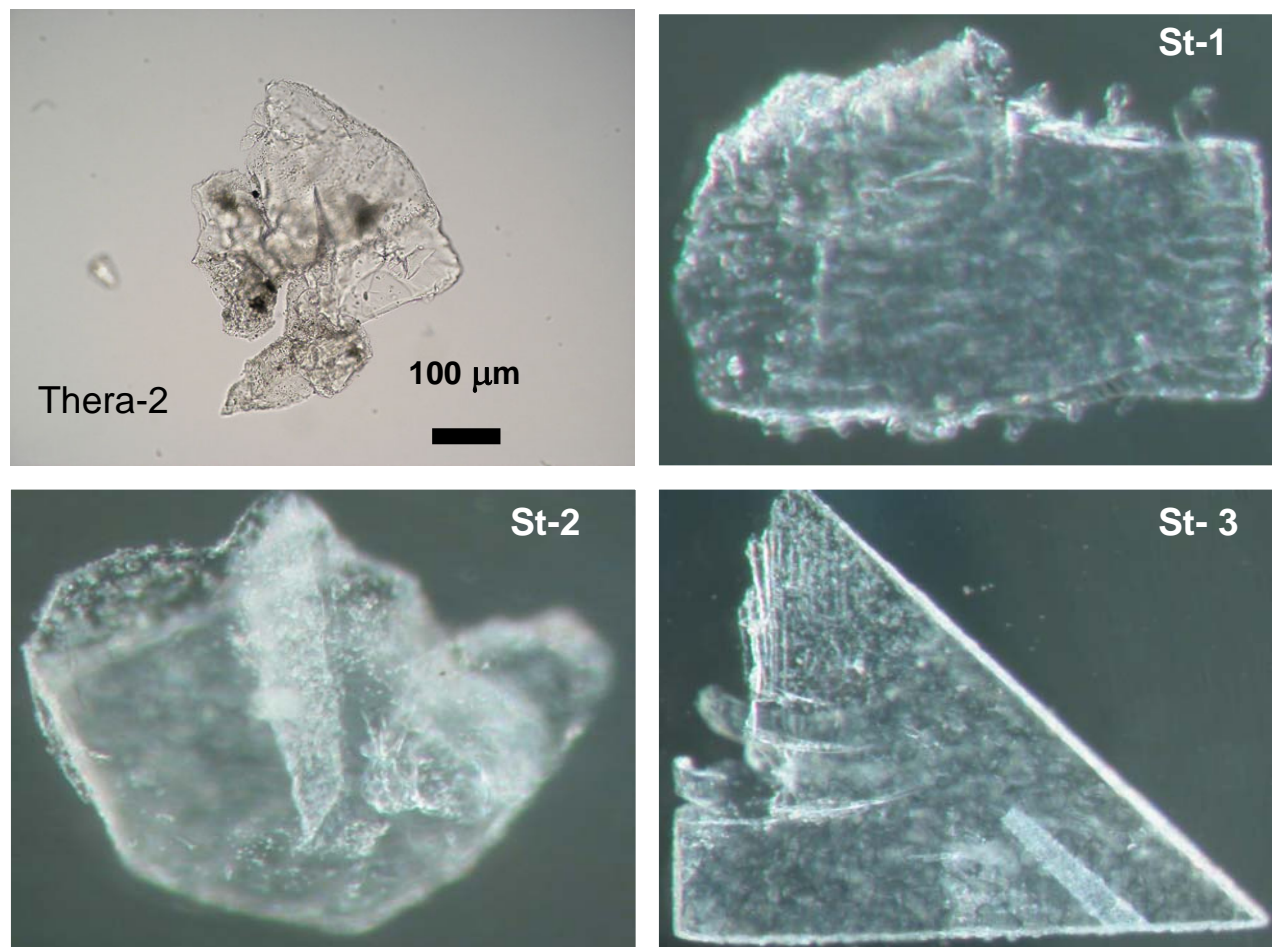


Fig. S1. Stardust samples Thera-2 (CRPG Nancy) and St-1, St-2, St-3 (University of Minnesota) extracted from the bulbous cavity wall of track #41, aerogel cell C2044. Thera-1 is shown in Fig. 1B, main text. Actual cavity-wall materials occupy only small areas of the pictured aerogel tiles. The Minnesota samples are ~1mm in largest dimension.

Methods

1) CRPG Nancy

Stardust samples were provided by the Isotope Preliminary Examination Team (PET) led by K. McKeegan (*S1*). We received blank aerogel chips, flown aerogel chips and two fragments of bulbous aerogel. The first piece was extracted as an aerogel "keystone" (*S2*) from the wall of a large bulbous track (track #41, cell C2044). This sample will be referred to in the following as Thera-1 (Fig. 1B, main text). This sample, together with blank and flown samples, were analyzed

after extensive blank determination (see below). Given the results of the first allocation, a second allocated larger piece of the same wall (Thera-2) was analyzed together with another piece of flown aerogel (Fig. S1).

Aerogel fragments were handled in a clean room (class 10,000 in the room, class 100 in extraction boxes) under a microscope using a clean single-hair paintbrush attached to a manipulator. It was not possible to weigh aerogel chips due to their small size, and we have estimated optically the surface area of the chips. Assuming that all chips have a comparable thickness, the surface area of a sample gives a first order idea of the aerogel sample quantity. Samples were loaded in pits of a laser cell in operation at CRPG Nancy, which was connected to a high vacuum line and baked at 80°C (Thera-1 run) and 100°C (Thera-2 run) overnight. The samples were then left under vacuum (1.5×10^{-9} mbar) at room temperature for 3 weeks (Thera-1) and 1 week (Thera-2), respectively.

Samples were heated using a CO₂ infrared ($\lambda = 10.6 \mu\text{m}$) laser mounted on an x-y stage and monitored through a microscope equipped with a CCD camera. We used a visible (He-Ne) laser to point samples and discovered that even the weak pointer laser provoked vibrations of the fragments under illumination. Hence we heated the chips with great care by very slowly increasing the power of the CO₂ laser in order to avoid samples jumping out of the pits. We lost one blank aerogel sample and did not analyze other small blank aerogel samples. Fortunately, the flown aerogel chips and the bulbous chips were bigger and could be safely analyzed. Once thermal coupling of the aerogel sample with the laser beam was achieved, aerogel chips could be totally melted.

Extracted gases were handled in a new facility at CRPG developed for the analysis of very low amounts of noble gases and nitrogen implanted in Genesis target material. Gases were cleaned up with two Ti sponge getters (one at 650°C, the other at room temperature), and analyzed in two fractions, He plus Ne, and Ar, with a VG5400 Micromass[©] static mass spectrometer (S3). The blanks were thoroughly investigated and analyses started only when the blanks were indistinguishable from those of the purification line alone, as determined during several months prior to these experiments. Blanks measured without the laser on, and with the laser illuminating a metal surface adjacent to the samples, were indistinguishable. The blank values ($n = 6$) were $1.1 \pm 0.6 \times 10^{-10}$, $1.9 \pm 0.4 \times 10^{-11}$, and $2.4 \pm 0.7 \times 10^{-12}$ cm³ STP for ⁴He, ²⁰Ne, and ³⁶Ar respectively. The amounts of argon released during sample runs were indistinguishable from those of the blank runs.

In all cases, blank corrections were critical. Potential sources of blank are (i) instrumental blank, determined without heating a sample, and (ii) the aerogel. The former should be approximately constant over a given period, whereas the latter should be proportional to the size of the aerogel sample. Fig. S2 represents the amount of He and Ne during the various runs as a function of the aerogel surface area for each sample. If (ii) was dominant, one would expect a correlation. On the contrary, if most of the blank is instrumental, there should not be any relationship between the aerogel chip size and the blank. Extractions of flown aerogel without bubbles are comparable to the blanks (represented by the shaded area in Fig. S2), given uncertainties. This suggests strongly that the instrumental blank dominates over the aerogel blank for the sample sizes we analyzed.

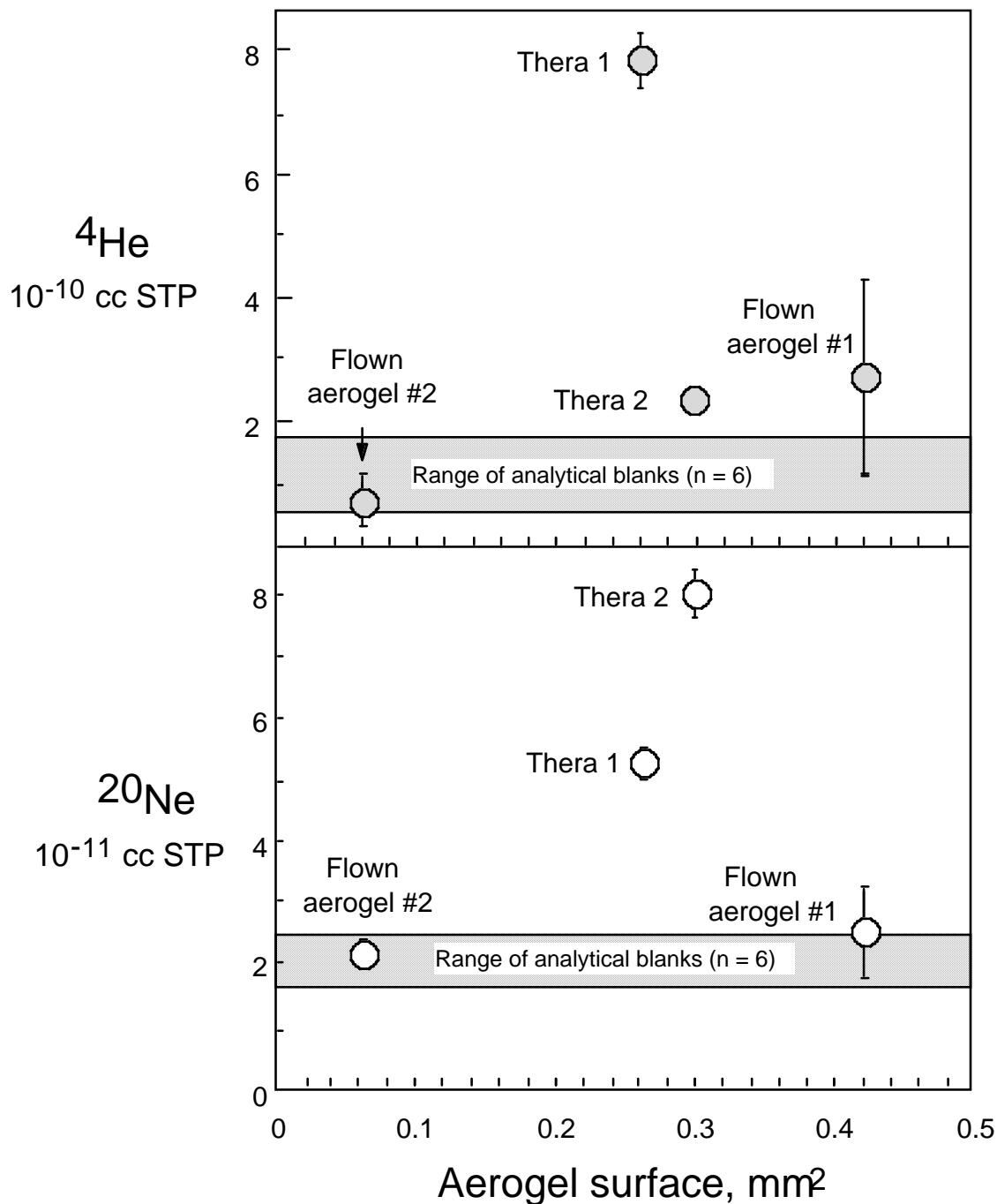


Fig. S2. He and Ne amounts extracted from aerogel chips of variable sizes (CRPG Nancy). The shaded areas represent the range of blank values for the analytical facility. There is no correlation between the amounts of He and Ne and the aerogel sample surface, strongly suggesting that the main source of blank is not the aerogel itself. Flown aerogel has He and Ne blanks undistinguishable from the procedural one. “Thera” samples have He and Ne contents clearly above the system blanks.

2) University of Minnesota

Three different sample types were analyzed: **(i)** A $\sim 1.5 \text{ mm}^2$ sample cut from a block of Stardust flight spare aerogel (E226-5B) supplied by M. Zolensky (Astromaterials Research and Exploration Science, NASA-Johnson Space Center) to determine the feasibility of measuring noble gases in particles embedded in aerogel. **(ii)** A blank sample $\sim 1.5 \text{ mm}^2$ in area (keystone CO44) of Stardust flight aerogel excised from an aerogel cell containing no visible cometary material, provided by the PET for further aerogel blank measurements. **(iii)** Three samples of aerogel-embedded cometary material (Fig. S1) extracted (S2) from the same bulbous track wall (track #41, cell C2044) distributed to the CRPG Nancy group, allocated to Minnesota by the PET to enable independent measurements in two laboratories. These samples are designated St-1, St-2, and St-3.

Samples were wrapped in Pt foil packets and attached across electric power leads in a miniature vacuum furnace. Following a 150-200 °C bakeout (all samples except St-3; see below), gases were extracted by stepped heating to $\sim 1075^\circ\text{C}$ at computer controlled power levels, with 15 or 20 second dwell times at each temperature, in a technique similar to that used for lunar grains (S4) and IDPs (S5). Gas release temperatures were repeatedly monitored by optical pyrometer, with an uncertainty of $\pm 50^\circ\text{C}$. Except for temperatures above $\sim 1075^\circ\text{C}$, there were only minor modifications of the computer controlled pulse heating procedures described in (S4). Three initial sequential heating steps at increasing power heated the samples to $\sim 250^\circ\text{C}$. Although the gases liberated in these steps were analyzed isotopically, the heating served primarily as a clean-up procedure to remove any surface sited or adsorbed gases not removed during the bakeout. Helium and Ne released in these steps was at or below the system blank levels described below. Up to 10 sequential heating steps at increasing power were then applied, resulting in step degassing temperatures ranging from ~ 250 to $\sim 1075^\circ\text{C}$. Cumulative release of ^4He and ^{20}Ne was monitored during the degassing. No He or Ne signals above blank levels were seen up to the maximum temperature ($\sim 1075^\circ\text{C}$) reached by the computer controlled system (Fig. S3). An external power supply was subsequently used to manually increase the temperature above 1075°C while monitoring the Pt packet temperature with an optical pyrometer. St-1 began to degas above blank levels at $\sim 1250^\circ\text{C}$, and St-2 and St-3 at $\sim 1300^\circ\text{C}$. Heating was terminated for all samples at $\sim 1400^\circ\text{C}$, the maximum attainable temperature for the Stardust Pt foil packets.

The loading and bakeout of St-3 were handled slightly differently than for St-1 and St-2. Because of the possibility that the samples might contain a gas component released at low temperatures that would have been lost from St-1 and St-2 during bakeout, there was no bakeout following the loading of St-3 into the gas extraction system. Despite this, the He and Ne signals observed during the low temperature ($< 250^\circ\text{C}$) and computer controlled heatings up to $\sim 1075^\circ\text{C}$ were still indistinguishable from blank values.

Earlier studies of flight spare aerogel with a residual gas analyzer had revealed large background abundances of H, H_2O , CO and CO_2 , so evolved gases were continually purified by a room temperature Westinghouse[®]/WL getter and cryopumped at LN_2 temperature. No attempt was made to measure Ar, whose abundance was anticipated to be undetectable above background. Helium and Ne were analyzed statically in a 3.75" double focusing Mattauch-Herzog geometry mass spectrometer equipped with pulse counting detectors, an instrument specifically designed for high sensitivity analyses of trace amounts of noble gases (S6). The mass spectrometer was

cryopumped at LN₂ temperature during all analyses. Signals at masses 18 (H₂¹⁶O), 40 (⁴⁰Ar), and 44 (¹²C¹⁶O₂), measured along with the Ne isotopes, were very low. Additionally, Ne was analyzed at an ionizing energy of 35eV, experimentally determined to be low enough that doubly ionized ⁴⁰Ar and CO₂ were undetectable at Ne masses 20 and 22. As a result, corrections to the Ne isotopic values consisted only of the H₂¹⁸O⁺ correction to mass 20. These ranged from 3.7% of the mass 20 abundance for the sample with most Ne (St-1) to 13-19% for St-2 and St-3.

Sensitivities for He and Ne were derived from repeated analyses of air samples metered into the system from calibration cans designed to permit accurate volumetric splitting, with non-noble gases removed by gettering and freezing out on charcoal at LN₂ temperature. Detection limits for the mass spectrometer used in this study were approximately 1×10^{-14} , 6×10^{-13} , and 2×10^{-13} cm³ STP for ³He, ⁴He, and ²⁰Ne, respectively.

Accurate measurements of blank levels were critical for the Stardust analyses. Aerogel volatiles may be separated into gas from the Stardust grains, and gas from all other sources. Gases intrinsic to aerogel itself may lie on surfaces and/or be trapped within the aerogel. To examine possible intrinsic noble gas sources, a ~1.5 mm² sample [(i) above] from flight spare block E226-5B was heated in nine 15 s steps from 300 to 1330°C and then reheated using the same procedures. Reheated values determined the system blank. All reported blank abundances are cumulative over the given temperature ranges. In the initial heating, the ⁴He abundance was 3.4×10^{-11} cm³ STP below 1000°C, increasing at 1330°C to 6.9×10^{-11} cm³ STP. In the reheat, the ⁴He abundance was 5.1×10^{-11} cm³ STP, whereas ³He and ²⁰Ne were indistinguishable in the initial and reheat runs (at $\sim 1.3 \times 10^{-14}$ and $\sim 6.6 \times 10^{-12}$ cm³ STP, respectively). These data suggested that a small intrinsic ⁴He component might be present in the aerogel, but show no evidence for intrinsic ³He or ²⁰Ne.

Blank analyses were repeated for the flight aerogel keystone C044 [(ii) above]. It was initially heated to 200°C for 20 s to release contamination loosely trapped in the sample or sample holder, then heated in three 15 s steps at 1140, 1250, and 1330 °C, with cumulative gas measurements taken after the final heating step. ³He, ⁴He and ²⁰Ne abundances were indistinguishable between cold blanks (no heating), the 200°C heating, the 1330°C initial heating, and a 1330°C reheating (system blank) at approximately 1.2×10^{-14} , 1.4×10^{-11} , and 2.4×10^{-12} cm³ STP, respectively. Thus, as observed earlier in the flight spare aerogel, there was no evidence for any ³He or ²⁰Ne intrinsic to the aerogel above system blank values. Moreover, in contrast to the flight spare aerogel, the Stardust flight aerogel yielded no detectable intrinsic ⁴He, and overall system blanks were lower.

Blanks, both cold and hot, were run on empty Pt foils. Duplicate reheats were also done on every sample. Since the clearest indication of non-terrestrial helium was the presence of an unambiguous ³He signal, utmost care was taken to evaluate the ³He blank value accurately. Seventeen ³He blank determinations were made throughout the sample analysis period. The values obtained were extremely consistent [$(1.20 \pm 0.08) \times 10^{-14}$ cm³ STP] and did not depend on the heating conditions of the run—time, temperature, or number of steps—but were instead dominated by counting statistics. This blank contributed 35% (St-1 and St-3) to 48% (St-2) of the ³He liberated during the high temperature sample analyses (Fig. S3).

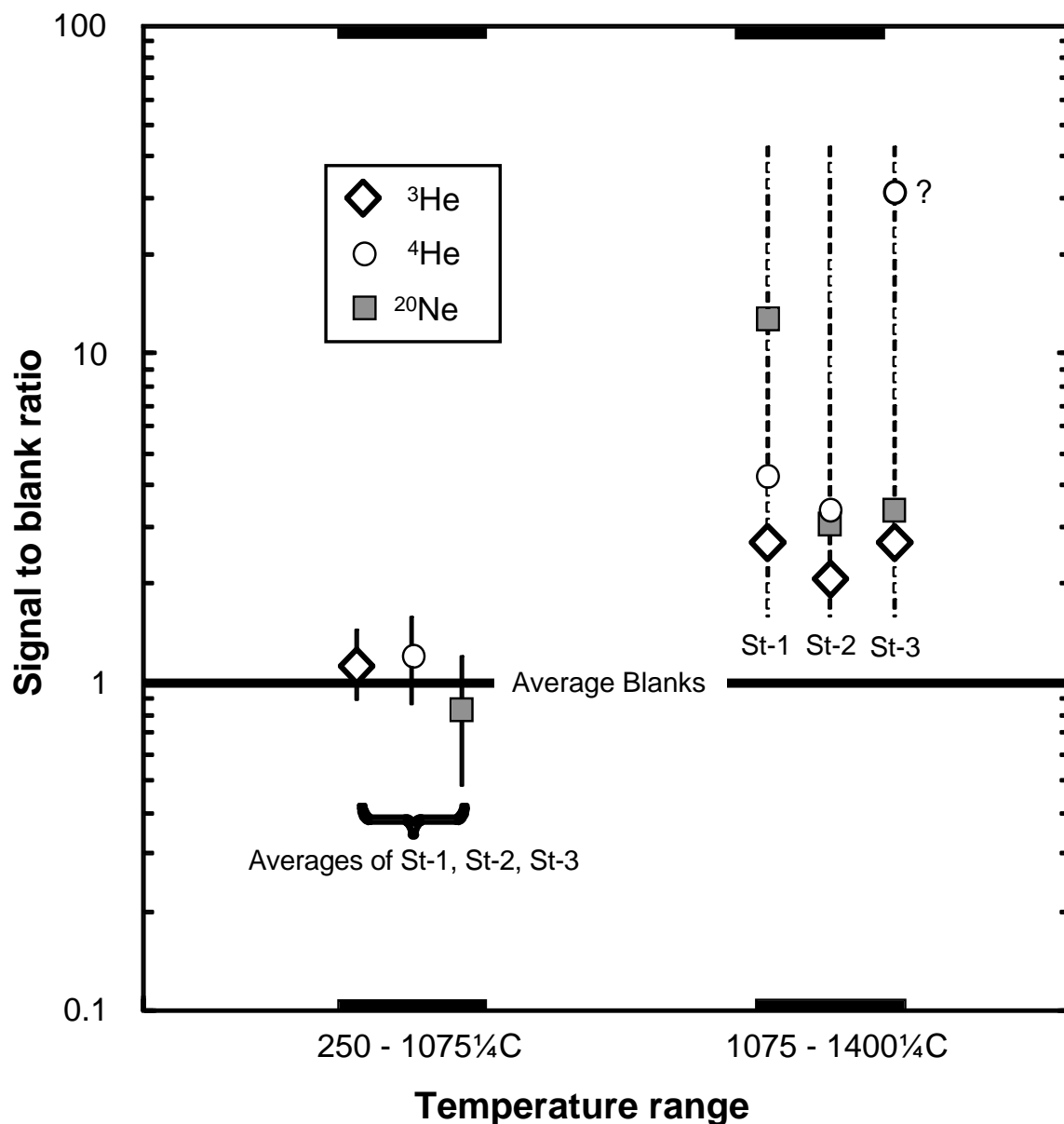


Fig. S3. Signal to blank ratios for cumulative releases of ³He, ⁴He, and ²⁰Ne from samples St-1, St-2, and St-3 (Minnesota) during step-heating from 250°C to 1075°C, and from 1075°C to 1400°C. Sample abundances evolved over the lower temperature range are indistinguishable from cumulative blank levels over the same range. High temperature gas release above blank levels commenced at ~1250 °C for St-1, and at ~1300 °C for St-2 and St-3. Errors on sample abundances include measurement uncertainties and, for the lower temperature data, scatter around the averages of the three samples. All errors are SEM. They are smaller than the symbol sizes for the high-temperature data. The high-temperature ⁴He abundance in St-3 is questionable because of a suspected high blank. Average cumulative blank abundances in Fig. S3, in cm³ STP, are $1.20 \pm 0.08 \times 10^{-14}$, $1.4 \pm 0.5 \times 10^{-11}$, and $2.4 \pm 0.6 \times 10^{-12}$ for ³He, ⁴He, and ²⁰Ne respectively over the 250-1075°C heating range, and $1.20 \pm 0.08 \times 10^{-14}$, $2.2 \pm 0.4 \times 10^{-11}$, and $4.4 \pm 1.2 \times 10^{-12}$ over the 1075-1400°C range.

As a result of their dependence on the heating conditions of the run, and thus having fewer overall blank measurements, ^4He and Ne blank corrections have greater associated error than those for ^3He . Only high temperature heatings similar to those releasing sample gas were used in determining the ^4He and Ne blanks, since in those instances a greater blank was consistently observed. In the case of ^4He , the average blank abundance of $(2.17 \pm 0.36) \times 10^{-11} \text{ cm}^3 \text{ STP}$ represented 23% (St-1), 29% (St-2), and 3% (St-3) of the ^4He liberated during the high temperature sample analyses, whereas for ^{20}Ne , the average blank of $(4.4 \pm 1.2) \times 10^{-12} \text{ cm}^3 \text{ STP}$ represented 8% (St-1), 32% (St-2) and 29% (St-3) of the ^{20}Ne released (Fig. S3).

The reheat ^4He blank level for sample St-3 was anomalously high, ~ 4 times the average given above for all other ^4He blanks. The gas released in the reheat was probably not from the sample since the ^3He value equalled the blank. The high ^4He gas abundance (and correspondingly low $^3\text{He}/^4\text{He}$ value compared to St-1 and St-2) observed in St-3 is therefore most likely due to evolution of extraneous ^4He from a sample holder assembly for St-3 which had not been completely degassed of contaminant air He prior to loading. It was released only at the highest temperatures, since the sample was heated to $\sim 1075^\circ\text{C}$ earlier with no liberated gas observed above blank. Suspicion about the validity of the measured ^4He abundance in St-3 is reflected in Table 1 (main text), where the ^4He gas abundance and $^4\text{He}/^{20}\text{Ne}$ ratio are listed as upper limits, and the $^3\text{He}/^4\text{He}$ as a lower limit. The ^3He abundance of $2.13 \times 10^{-14} \text{ cm}^3 \text{ STP}$, however, is comparable to those in St-1 and St-2 (2.12×10^{-14} and $1.30 \times 10^{-14} \text{ cm}^3 \text{ STP}$ respectively).

Supporting Text

1) Bulb-wall Mineralogy and Grain Masses: Space Sciences Laboratory, University of California Berkeley

We analyzed captured cometary material in track 41 using synchrotron-based microbeam X-ray Fluorescence and X-ray Near-Edge Absorption Spectroscopy (XANES), utilizing the μXANES beamline 10.3.2 at the Advanced Light Source, Lawrence Berkeley Laboratory. The synchrotron x-ray beam was focused to a beamspot several microns in diameter by Kirkpatrick-Baez mirrors, and tuned in energy using an upstream monochrometer. The energy width of the monochromatic beam was $\sim 1 \text{ eV}$. The track was extracted from its aerogel tile using the "keystoning" technique (S2). The block of aerogel, measuring 4.5mm x 9.5 mm x 11 mm, completely contained the track and terminal particles. To determine the mineralogy of the Fe-bearing phases, 32 grains or grain clusters in the track bulb wall were analyzed using Fe XANES. Here we scanned in energy across the K-edge of Fe, and fit the normalized spectrum using non-negative linear least squares to a reference library consisting of 83 reference spectra from 54 different minerals in 24 different mineral groups (metal, sulfide, carbide, olivine, orthopyroxene, clinopyroxene, glass, and others). While there can be strong degeneracies between individual minerals within groups, identification of mineral families is generally reliable. This assay yielded the following average distribution of total Fe, in atom%, among identified mineral constituents in the bulb wall: 9% in metal, 51% in sulfides, 24% in carbides, and 16% in silicates, glasses, and other (unidentified) constituents. The corresponding mass distributions are 6 wt.% metal (with metal taken to be Fe), 53 wt.% sulfides (as FeS), 17 wt.% carbides (as Fe_3C), and 24 wt.%

silicates + other (with an atom% composition assumed to be the CI composition listed in Table 1 of (S7)). The two large particles (~10-15 μm) lodged at track termini (Fig. 1A, bottom) are FeNi (kamacite). The incident Stardust particle was clearly rich in iron and iron-sulphur compounds such as troilite and pyrrhotite. Silicates in addition to those detected could also be present since end member (Fe-free) olivines and enstatite are invisible to Fe XANES. However many low-Fe Stardust olivines contain significant Ca (*I*) which would be seen in the measurements. Such Ca-bearing phases were rare.

The mass of Fe in the track bulb was estimated by comparing background-subtracted Fe $K\alpha$ fluorescence to that of a scan of the NIST 1833 standard film using identical parameters (11 keV beam energy, 100ms dwelltime per pixel, $5\mu\text{m} \times 5\mu\text{m}$ pixel size). Corrections were made for attenuation of the fluorescence photons due to absorption in the aerogel block containing the track. The measurements gave an Fe mass of 26 ng in the projected bulb-wall area of $3.6 \times 10^{-2} \text{ cm}^2$. Multiplication by π converted the projected area to the actual bulb-wall area (assumed approximately cylindrical) of 0.113 cm^2 , resulting in an average areal Fe density of 230 ng/cm^2 . The mineral speciation given above for Fe yielded elemental masses/ cm^2 of S (67 ng), C (4 ng), O (26 ng), Mg (8 ng), and Si (11 ng), for a total bulb-wall grain mass of $\sim 350 \text{ ng/cm}^2$. The average area of bulb-wall material in each of the 5 samples analyzed for noble gases was calculated in two ways: (a) from the area of bulb wall material contained in each sample, estimated from the sample images in Figs. 1B and S1; and (b) from the total wall area contained in the excised keystone —assumed to be equally partitioned into the 5 samples— obtained by direct measurements on the keystone quarry seen in Fig. 1A. The two calculations agreed to $\pm \sim 10\%$ and gave an average of $\sim 7.3 \times 10^{-4} \text{ cm}^2$ per sample. The average grain mass per sample is then $\sim 0.26 \text{ ng}$.

2) Bulb-wall Organics: Lawrence Livermore National Laboratory

Measurements of organic components in an aerogel sample of the track 41 bulb wall, cut under an angle to the particle track, were obtained with Fourier transform infrared (FTIR) microscopy at the Advanced Light Source (ALS), Lawrence Berkeley National Laboratory. The non-invasive nature of IR spectroscopy and high sensitivity to chemical functional groups makes this an ideal technique for fingerprinting. A typical measurement records a spectrum of IR absorbance in the sample as a function of the wavelength. The basic principle is that the IR light is being absorbed only if the frequency matches exactly the frequency of the vibrational mode of a chemical functional group and the vibration causes an asymmetric change in the charge distribution within the molecule (dipole moment). Atoms of a molecule vibrate with characteristic frequencies (normal modes) governed by their chemical bonds and symmetry environment. Vibrational mode sets are unique for every molecular configuration. FTIR measurements have successfully detected organic compounds in thin TEM sections of Stardust particles and by mapping of whole keystones with particle tracks (S8, S9).

Although the FTIR microscope is attached to the synchrotron source, an internal source was used for these particular measurements. With a small aperture, this source has a good signal-to-noise ratio with $\sim 40 \mu\text{m}$ lateral resolution. The SpectraTech Nic-Plan IR microscope at the ALS beamline is equipped with a ThermoNicolet Magna 760 FTIR bench. A KBr beamsplitter was

placed in the beam path and the transmitted light was collected with a MCT-A detector between 650 and 4000 cm^{-1} with 4 cm^{-1} spectral resolution. Spectra were normalized to the spectrum of the beam through the air and typical collection times were between 12 and 256 seconds per point. The sample was placed on a sub-micron precision microscope stage and measured in air after the optical and infrared beams were co-aligned.

A ~ 200 μm thick slice of aerogel cut across the particle track was mounted between two metallic foils with a small hole. IR analyses were carried out both in and adjacent to the track wall and, for blank corrections, hundreds of microns away from the track wall. Measured blank-corrected areal densities of the $-\text{CH}_2$, $-\text{CH}_3$, and $\text{C}=\text{O}$ functional groups in the bulb wall, in number/ cm^2 , were $<9.1 \times 10^{10}$, 1.6×10^{11} , and $<1.4 \times 10^{11}$ respectively. The corresponding hydrocarbon mass, calculated from the measured densities and the molecular weights of the functional groups, is <13 pg/cm^2 . IR mapping at distances ≥ 50 μm outside the wall detected no labile organics diffused into the adjacent aerogel, a distribution commonly seen around organic-rich tracks (*S8*). These measurements suggest a very low organics content in track 41, as observed in some other Stardust tracks (*S8*). Extended to the present samples, multiplication by the average area of bulb-wall material in each of the 5 samples, estimated above to be $\sim 7.3 \times 10^{-4}$ cm^2 , yields an average organic abundance per sample of <10 fg. Lower limits on ^{20}Ne and ^4He concentrations, from this mass and average gas abundances per sample from Table 1 (main text), would then range from >3000 $\text{cm}^3\text{STP}/\text{g}$ to >20000 $\text{cm}^3\text{STP}/\text{g}$ respectively if the gases were hosted in this amount of organic matter. Trapping at such levels is clearly implausible, and would remain so even if the masses of functional groups not included in the FTIR survey (e.g., C-N, C=C) exceeded the measured upper limit by an order of magnitude or more. However only a few percent of the total wall and exterior of the large track 41 were mapped in this survey, so the possibility remains that higher levels of inhomogeneously distributed organics could be present in other sections of the track wall and adjacent aerogel.

3) Spallation Production of ^3He and ^{21}Ne

Production rates of ^3He and ^{21}Ne by GCR-induced spallation reactions are maximum in the upper meter or so of an irradiated body, and fall off rapidly with increasing depth. Particles exposed to GCR radiation at these near-surface locations thus require minimum residence times in order to accumulate a given inventory of spallogenic nuclides. Applied to Wild 2, the GCR production rate of ^3He in a particle with the composition given above is $\sim 5.6 \times 10^{-9}$ $\text{cm}^3\text{STP}/\text{g}$ per Ma if residing on the surface, and $\sim 3.3 \times 10^{-9}$ $\text{cm}^3\text{STP}/\text{g}$ per Ma if buried to a depth of 1 m in cometary ices. Production rates were calculated from element-specific spallation yields as functions of depth in a large body (*S10*), where S yields were interpolated between those for Si and Fe since S is not included among the target elements tabulated in (*S10*). With an average ^3He loading of $\sim 7.1 \times 10^{-5}$ $\text{cm}^3\text{STP}/\text{g}$ in the cavity-wall samples (main text), GCR exposures of ~ 6300 Ma at zero depth or ~ 11000 Ma at 1 m would be needed to generate half the observed ^3He and thus elevate $^3\text{He}/^4\text{He}$ from the Q-He ratio to its measured values; both residence times exceed the 4500 Ma age of the solar system. A similar calculation using ^{21}Ne production rates (*S11*) yields a spallogenic contribution of $<1\%$ of the measured ^{21}Ne at either location.

4) Diffusion Calculations and Gas Acquisition Modelling

In response to a suggestion by a reviewer that our observed He and Ne isotopic and elemental ratios might have been derived from a solar composition reservoir by fractionation during a loss process, we have calculated the isotopic fractionations that would result for He and Ne due to Fick's Law diffusion from a spherical particle (for a range of radii between 1 and 75 μm) of a component with a uniform initial distribution in the grain (as would result from trapping from a gas reservoir during grain formation), and of a component present in a thin shell of a few hundred \AA depth on the surface of such spherical grains (as would result from a solar wind-like ion irradiation). We also calculated the fractionations that would be generated by Rayleigh distillation of He and Ne from a well-mixed gaseous reservoir, prior to the possible incorporation of such gases into a Stardust particle, and allowing for possible gas diffusion rate-relationships for isotopic pairs other than square root of mass —i.e., gas loss processes more complicated than simple diffusion into a vacuum.

In all of these cases the fractional losses required to fractionate the $^3\text{He}/^4\text{He}$ and $^{20}\text{Ne}/^{22}\text{Ne}$ ratios from solar to the observed ratios were larger for ^{22}Ne than for ^4He , usually by about an order of magnitude. This cannot happen in a Rayleigh distillation, where fractional escape decreases with increasing mass. If such fractionations occurred in diffusive losses from a solid grain, they would require that the diffusion coefficient for He in the grain was much less than that for Ne, and we would expect to measure a $^4\text{He}/^{22}\text{Ne}$ ratio above the solar value. Since the observed $^4\text{He}/^{20}\text{Ne}$ ratio is fractionated from the solar ratio by about two orders of magnitude in the opposite direction to the calculation, and since diffusion coefficients in natural solids are expected to be greater for He than for Ne, we conclude that the measured isotopic and elemental ratios could not have been derived from a solar composition precursor by normal physical processes.

Although for these reasons it does not appear possible to derive Stardust compositions directly from an initially solar-like reservoir, an alternative two-stage scenario of gas acquisition and diffusive fractionation, which does call for the presence of a component emitted by the early Sun, seems capable of replicating observed He and Ne distributions. Grains carrying Q-gases possibly implanted by ion irradiation in a hot plasma subsequently experience large diffusive losses, primarily of He; Ne isotope ratios are essentially unaltered. At some later time they are exposed to radiation from the early sun that implants a post D-burning solar gas component, elevating the highly diffused $^3\text{He}/^4\text{He}$ and $^4\text{He}/^{20}\text{Ne}$ ratios with only minor effect on Ne since solar He/Ne is so high (Table S1). This scenario, while speculative, can reproduce the measured He and Ne compositions, including the anomalously low $^4\text{He}/^{20}\text{Ne}$ ratios.

Results of an example calculation are given in Table S1. Diffused Q-He and Q-Ne compositions were calculated by applying Fick's Law to a spherical grain initially uniformly loaded with Q-gases. In view of the mineral composition of the Track 41 particle given above, the grain was assumed to be dominantly metallic. The ratio of diffusion coefficients $D(\text{He})/D(\text{Ne})$ was taken to be 10, an approximate value for diffusion from iron at temperatures of $\sim 500\text{-}1000\text{ K}$ (S12). With this ratio the diffusive loss factor $f(^{20}\text{Ne})$ and fractionation of Ne isotope ratios from their values in the undiffused Q component are small (Table S1). The solar contribution to the final "Diffused Q + Solar" mixture is $\sim 50\%$ of the total ^4He but $<1\%$ of the total ^{20}Ne , so adding the solar component has little effect on Ne abundance and isotope ratios (Table S1). We have used the

present solar-wind $^3\text{He}/^4\text{He}$ ratio in the calculation, but with higher diffusive He loss ($f(^4\text{He}) = 77$) the lower estimate for the post D-burning ratio in the Sun (Fig. 2B, main text) can be accommodated. A final $^4\text{He}/^{20}\text{Ne}$ ratio of 10, an approximate average of the measured Stardust ratios, is obtained in this example; higher or lower degrees of Q-gas diffusion can replicate the observed range of ~ 1 -20. The diffusion coefficient ratio $D(\text{He})/D(\text{Ne})$ is constrained to be >5 for all solutions. With smaller ratios, Ne loss is large enough to fractionate $^{20}\text{Ne}/^{22}\text{Ne}$ to values below the Stardust measurement uncertainties.

Table S1. Comparison of Stardust measurements with He and Ne compositions generated by a mixture of diffused Q-gases with solar gases. The $f(^4\text{He})$ and $f(^{20}\text{Ne})$ entries are the factors by which the He and Ne initially present in the Q-carrier grain are diffusively depleted. Solar (solar wind) and undiffused Q compositions from Table 1, main text.

	$^3\text{He}/^4\text{He}$ ($\times 10^{-4}$)	$^{20}\text{Ne}/^{22}\text{Ne}$	$^{21}\text{Ne}/^{22}\text{Ne}$ ($\times 10^{-2}$)	$f(^4\text{He})$	$f(^{20}\text{Ne})$	$^4\text{He}/^{20}\text{Ne}$
Solar	4.44 ± 0.10	13.90 ± 0.08	3.35 ± 0.07			520 - 670
Undiffused Q	1.45 ± 0.15	10.10-10.70	2.78-2.94			110 ± 30
Diffused Q	0.876	9.88-10.46	2.75-2.91	47	2.2	4.9
Diffused Q + Solar	2.75	9.90-10.49	2.75-2.91			10
Stardust	2.75 ± 0.21	10.55 ± 0.20	2.77 ± 0.14			~ 1-20

References

- S1. K. D. McKeegan *et al.*, *Science* **314**, 1724 (2006).
S2. A. J. Westphal *et al.*, *Meteorit. Planet. Sci.* **39**, 1375 (2004).
S3. B. Marty, P. Robert, L. Zimmermann, *Meteorit. Planet. Sci.* **40**, 881 (2005).
S4. R. L. Palma, R. O. Pepin, R. Becker, D. J. Schlutter, *Geochim. Cosmochim. Acta* **66**, 2929 (2002).
S5. R. L. Palma, R. O. Pepin, D. J. Schlutter, *Meteorit. Planet. Sci.* **40**, A120 (2005).
S6. A. O. Nier, D. J. Schlutter, *Rev. Sci. Instr.* **56**, 214 (1985).
S7. M. E. Zolensky *et al.*, *Science* **314**, 1735 (2006).
S8. S. A. Sandford *et al.*, *Science* **314**, 1720 (2006).
S9. L. P. Keller *et al.*, *Science* **314**, 1728 (2006).
S10. R. C. Reedy, in *Proc. 12th Lunar Planet. Sci. Conf.*, *Geochim. Cosmochim. Acta Suppl.* **16**, pp. 1809-1823 (1981).

- S11. C. M. Hohenberg, K. Marti, F. A. Podosek, R. C. Reedy, J. R. Shirck, in *Proc. 9th Lunar Planet. Sci. Conf., Geochim. Cosmochim. Acta Suppl.* **10**, pp. 2311-2344 (1978).
- S12. H. Fechtig, W. Gentner, P. Lämmerzahl, *Geochim. Cosmochim. Acta* **27**, 1149 (1963).